Eur. Phys. J. A **20**, 173–178 (2004)
DOI 10.1140/epja/i2002-10347-6

THE EUROPEAN PHYSICAL JOURNAL A

Shape changes and test of the critical-point symmetry X(5) in N = 90 nuclei

A. Dewald[1,a], O. Möller[1], D. Tonev[1], A. Fitzler[1], B. Saha[1], K. Jessen[1], S. Heinze[1], A. Linnemann[1], J. Jolie[1], K.O. Zell[1], P. von Brentano[1], P. Petkov[2], R.F. Casten[1], M. Caprio[3], J.R. Cooper[3], R. Krücken[3,6], V. Zamfir[3], D. Bazzacco[4], S. Lunardi[4], C. Rossi Alvarez[4], F. Brandolini[4], C. Ur[4], G. De Angelis[5], D.R. Napoli[5], E. Farnea[5], N. Marginean[5], T. Martinez[5], and M. Axiotis[5]

[1] Institut für Kernphysik der Universität zu Köln, Köln, Germany
[2] Institute for Nuclear Research and Nuclear Energy Sofia, Sofia, Bulgaria
[3] W.N.S.L., Yale University, New Haven, CT 06520, USA
[4] Dipartimento di Fisica dell' Università and INFN Sezione Padova, Padova, Italy
[5] INFN, Laboratori Nazionali di Legnaro, Legnaro, Italy
[6] Physik-Department E12, TU München, Garching, Germany

Received: 30 October 2002 /
Published online: 2 March 2004 –

Abstract. Reliable and precise lifetimes of excited states in ^{154}Gd and ^{156}Dy were measured using the recoil distance Doppler shift (RDDS) technique. Excited states of ^{154}Gd were populated via Coulomb excitation with a ^{32}S beam at 110 MeV delivered by the FN Tandem accelerator at the University of Cologne. For ^{156}Dy a coincidence plunger experiment was performed at the Laboratori Nazionali di Legnaro with the GASP spectrometer and the Cologne coincidence plunger apparatus using the reaction ^{124}Sn(^{36}S,4n)^{156}Dy at a beam energy of 155 MeV. Shape changes previously suggested to appear in the ground-state band (gsb) of ^{156}Dy and in the s-band above the first band crossing were not supported by the transition probabilities determined in this work. The measured transition probabilities of ^{156}Dy and ^{154}Gd as well as the corresponding energy spectra are compared with the predictions of the recently proposed $X(5)$ model and in the case of ^{156}Dy also with an IBA fit.

PACS. 21.10.Tg Lifetimes – 27.70.+q $150 \leq A \leq 189$ – 21.60.Ev Collective models – 23.20.-g Electromagnetic transitions

1 Introduction

Nuclei with $N = 90$ have been investigated very extensively both experimentally as well as theoretically. A lot of spectroscopic data has been accumulated so far and many interesting phenomena, *e.g.*, band crossings, band terminations, and shape changes were investigated, *e.g.* [1–3]. The ground-state spectra of the $N = 90$ Nd, Sm, Gd and Dy nuclei are very similar, whereas the corresponding β deformations vary within $\beta = 0.27$–0.30. The transition quadrupole moments of the ground-state band (gsb) were found to increase slightly with spin. Surprisingly the Q_t values of ^{156}Dy differ from the pattern observed in the neighboring isotones. They follow a zig-zag curve which has been explained by assuming changes in the nuclear β and γ deformation [1]. The question for the cause of such an unexpected behavior has motivated a lifetime measurement as a stringent test to the previous experimental data. Another important motivation for the present experimental work was triggered by the introduction of the new $X(5)$ symmetry at the critical point of the $SU(3)$-$U(5)$ phase transition [4]. This new symmetry had experimentally been established in ^{152}Sm [5] and ^{150}Nd [6] for the first time. The neighboring $N = 90$ nuclei ^{154}Gd and ^{156}Dy were regarded as promising candidates to exhibit these characteristic $X(5)$ features, too.

2 Experimental details

In this paper we present the results of two lifetime experiments. One was performed at the FN Tandem accelerator of the University of Cologne using the recoil distance Doppler shift (RDDS) technique after Coulomb excitation of states in ^{154}Gd with a ^{32}S beam of 110 MeV. The target consisted of 1 mg/cm^2 of enriched ^{154}Gd evaporated onto a 2 mg/cm^2 Ta foil. The recoiling ^{154}Gd nuclei were stopped in a 5 mg/cm^2 Nb foil mounted together with the

[a] e-mail: Alfred.Dewald@ikp.Uni-Koeln.de

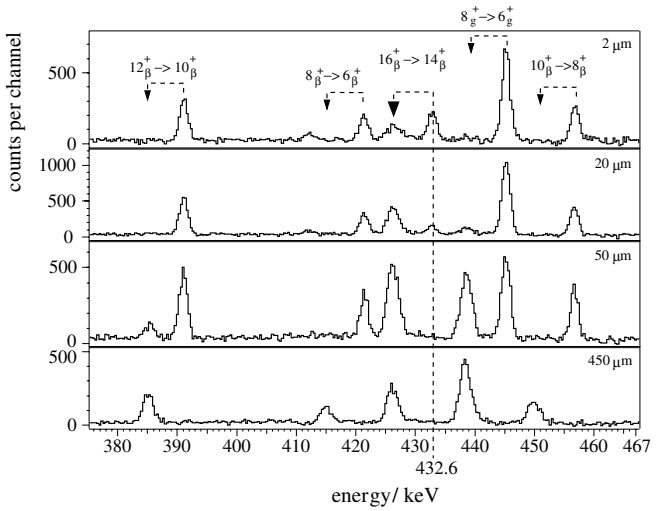

Fig. 1. Examples of gated spectra for different target-to-stopper distances.

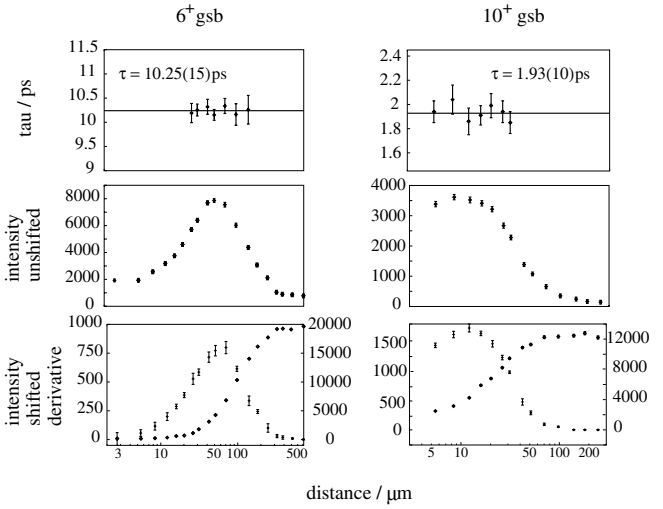

Fig. 2. Examples of τ-curves for the $6^+ \rightarrow 4^+$ and $10^+ \rightarrow 8^+$ transitions.

target in the Cologne coincidence plunger apparatus. In order to fix the kinematics of the reaction, backscattered, beam particles were detected by 6 Si detectors mounted downstream close to the target foil. The experimental set-up was very similar to that described in [7,8]. Particle gated singles spectra were analyzed and lifetimes of six excited states were determined using the differential decay curve method (DDCM) [9]. The results obtained are in good agreement with previous ones [10]. The lifetime of the 4_2^+ state which is important for the test of the $X(5)$ predictions was measured for the first time.

For ^{156}Dy a RDDS measurement was performed at the Laboratori Nazionali di Legnaro with the GASP spectrometer and the Cologne coincidence plunger. In addition, a Doppler shift attenuation measurement (DSAM) was done. The reaction ^{124}Sn(^{36}S,4n)^{156}Dy at a beam energy of 145 MeV was used for both experiments. Enriched ^{124}Sn targets of 1 mg/cm^2 and 0.9 mg/cm^2 thickness, evaporated onto 1.8 mg/cm^2 and 13.4 mg/cm^2 Ta backings, were used for the RDDS and the DSAM runs, respectively.

Figure 1 shows examples of gated spectra for different target-to-stopper distances.

The data were analyzed with the DDCM for $\gamma\gamma$ coincidence data [9,11] where the lifetimes are determined from the following equation:

$$\tau(x) = \frac{I_{\mathrm{su}}^{\mathrm{BA}}(x) - \alpha I_{\mathrm{su}}^{\mathrm{CA}}(x)}{\frac{\mathrm{d}}{\mathrm{d}x} I_{\mathrm{ss}}^{\mathrm{BA}}(x)} \frac{1}{v},$$

where

$$\alpha = \frac{I^{\mathrm{CA}}}{I^{\mathrm{CB}}} = \frac{I_{\mathrm{su}}^{\mathrm{CA}} + I_{\mathrm{ss}}^{\mathrm{CA}}}{I_{\mathrm{su}}^{\mathrm{CB}} + I_{\mathrm{ss}}^{\mathrm{CB}}},$$

x is the target-to-stopper separation and v is the recoil velocity.

The intensities $I_{\mathrm{su}}^{\mathrm{BA}}$, $I_{\mathrm{ss}}^{\mathrm{BA}}$ are the number of events where the shifted (s) component of a direct feeding transition B is coincident with the shifted (s) or unshifted (u) component of a depopulating transition A of the level of interest. The intensities for indirect feeding $I_{\mathrm{su}}^{\mathrm{CA}}$, $I_{\mathrm{ss}}^{\mathrm{CA}}$ are defined analogously.

The lifetimes of ^{156}Dy were obtained using gated spectra with gates from above the levels of interest alone. For the analysis those Ge detectors of GASP which are positioned at almost the same angles with respect to the beam axis, were grouped into 7 rings and the $\gamma\gamma$ coincidence events were sorted into different matrices corresponding to all possible combinations of these rings. The coincidence data of 4 rings, each containing 6 detectors with the polar angles of 34°, 59°, 121° and 146°, respectively, were used for the further lifetime analysis because only at these angles shifted and unshifted components can be distinguished in the corresponding spectra.

Lifetimes determined from different matrices are statistically independent and allow for a check of consistency. In addition, by using different gates, *e.g.* on direct or indirect feeders, more statistically independent lifetime values were obtained. The mean values of the different lifetimes determined for a specific level give the final result.

Since lifetimes τ are calculated for every flight time $t = \frac{x}{v}$, one obtains a function $\tau(t)$, the so-called τ-curve, which of course has to be a constant. Deviations from a constant behavior indicate the presence of systematic errors. Further details can be found in [9].

By gating from above the level of interest all problems related to discrete and unobserved feeders are eliminated. In addition, by gating only on the shifted component of a feeding transition the effect of deorientation cancels out completely [12]. Figure 2 shows examples of τ-curves obtained for the 6^+ and 10^+ states of the gsb of ^{156}Dy (upper panels). The middle panels show the corresponding intensities of the unshifted components. In the lower panel the shifted components are plotted *versus* the target-to-stopper distances as well as the corresponding derivatives of a depopulating transition.

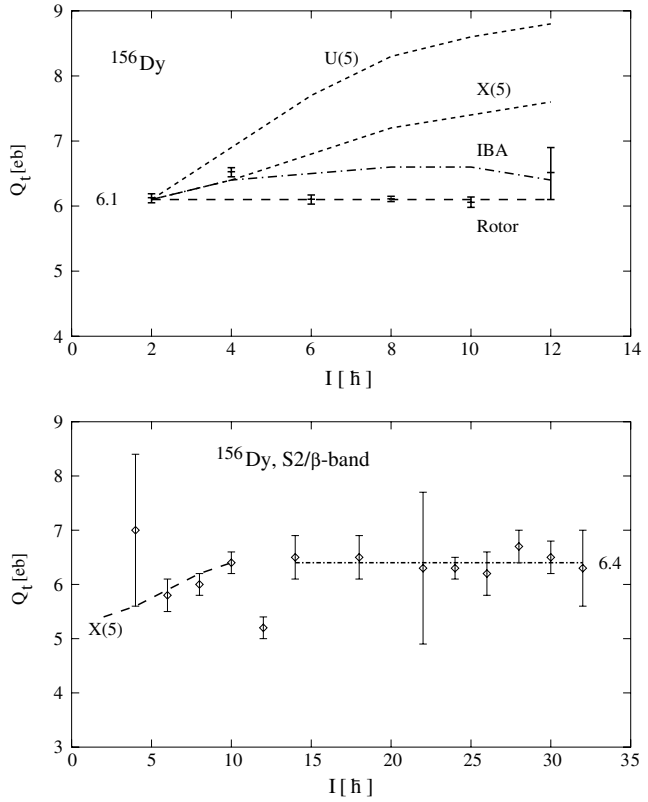

Fig. 3. Upper panel: Q_t values of the gsb of ^{156}Dy together with the theoretical values of the $X(5)$ symmetry, the symmetric rotor, the IBA $U(5)$ limit and an IBA fit normalized to the experimental $Q_t(2^+ \rightarrow 0^+)$ value. Lower panel: Q_t values of the β-band ($S2$-band) and above spin $12\hbar$ those of a s-band). The dashed line depicts the $X(5)$ values of the $S2$-band.

From the RDDS experiment 13 lifetimes were determined with experimental errors between 2 and 5%. From the DSAM analysis 6 lifetimes were obtained for the 22^+–32^+ states of the s-band. Because of a lack of statistics, only gates from below the level of interest were analyzed. For further details of the procedure employed and the used stopping power we refer to [13].

3 Discussion

3.1 Shape changes in ^{156}Dy

In the case of ^{156}Dy the results of this work differ partly from previous values. *E.g.*, for the 6^+ state we obtained a shorter lifetimes as given in [1,14]. The lifetimes of the 10^+ and 12^+ states were found to be longer. All DSAM results of this work are considerably shorter compared to previous results. Figure 3 shows the deduced Q_t values of this work for the gsb, β- and s-band. The values for the gsb follow the constant line representing the values of a symmetric rigid rotor with $Q_0 = 6.1$ eb. Only the Q_t value of the $4^+ \rightarrow 2^+$ transition is slightly above this value. Also shown are several theoretical values which are discussed below. The previously observed zig-zag pattern is not reproduced by our results. This holds also for the Q_t values in the s-band after the first band crossing of a $\nu(i_{13/2})^2$ quasiparticle band. The band crossing is exhibited by the reduced Q_t value of the $12^+ \rightarrow 10^+$ transition. Above the 12^+ state the Q_t values are again very constant with a mean value of $Q_t = 6.4$ eb.

Changes in the β and γ deformation as discussed in [1, 2] are not supported by the new data any more.

The Q_t values in the β-band increase with spin up to the point of the band crossing at spin $12\hbar$. This is discussed in the next section.

Table 1. Comparison of energy ratios of several $N = 90$ nuclei with the $X(5)$ values.

Energy ratios	^{150}Nd	^{152}Sm	^{154}Gd	^{156}Dy	$X(5)$
$E(4_1^+)/E(2_1^+)$	2.93	3.01	3.03	2.93	2.92
$R(4/2)_{S2}$	2.63	2.69	2.71	2.67	2.80
$E(0_2^+)/E(2_1^+)$	5.19	5.62	5.53	4.88	5.67

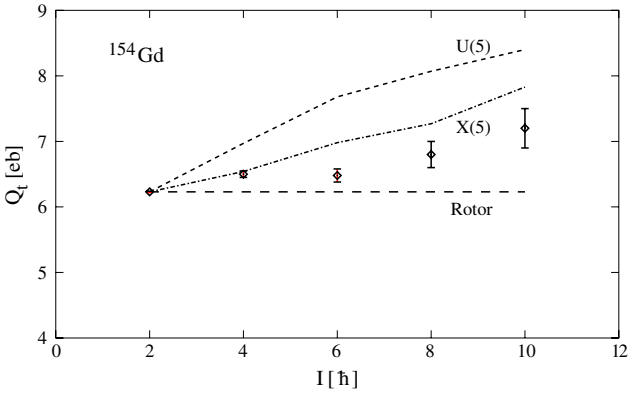

Fig. 4. Q_t values of the gsb of ^{154}Gd together with the theoretical values of the $X(5)$ symmetry, the symmetric rotor and the IBA $U(5)$ limit normalized to the experimental $Q_t(2^+ \rightarrow 0^+)$ value.

3.2 Critical-point symmetry X(5)

The possibility of investigating nuclear phase transition phenomena is one of the new and very challenging topics in nuclear-structure physics. A lot of theoretical and experimental work had been devoted to this topic and especially to the question on how phase transitions manifest in nuclei. [15,16,4,5,17–20]

Important contributions were made by F. Iachello who introduced the new dynamical symmetries $E(5)$ and $X(5)$ at the critical points of phase transitions between $U(5)$ and $O(6)$ and between $U(5)$ and $SU(3)$, respectively. The manifestation of these new symmetries allows the definition of specific experimental observables, needed to relate the theoretical picture with existing nuclei, and thus make a test of the theoretical concepts possible. Further work had been devoted to define phase transitions and critical points in finite quantal systems on an improved theoretical

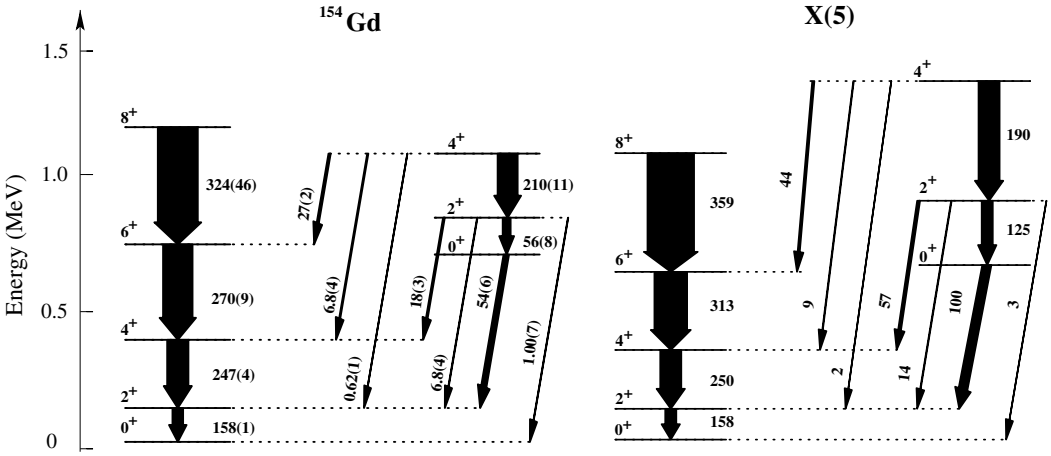

Fig. 5. Comparison of experimental data of ^{154}Gd with the $X(5)$ predictions. The $E(2_1^+)$ value (in keV) and the $B(E2; 2_1^+ \to 0_1^+)$ value (in W.u.) are normalized to the experimental data. The $B(E2)$ values are given next to the arrows.

basis, especially for nuclear shape phase transitions, by relating it to the Landau theory of continuous phase transition [21]. This work led to an extention of the so-called Casten triangle and includes explicitly oblate deformed nuclei [20]. This extended Casten triangle (fig. 7 below) can be considered as a phase diagram for nuclei with the IBM dynamical symmetries $U(5)$, $SU(3)$ and $\overline{SU(3)}$ located at the corners of the triangle. Three different phases (nuclear deformations) are contained in this triangle which are separated by the borderlines, representing first-order phase transitions between spherical and deformed phases and between oblate and prolate deformations. The dynamical symmetry $O(6)$ is located between $SU(3)$ and $\overline{SU(3)}$ and is considered to indicate a phase transition also. The new dynamical symmetry $E(5)$ appears to be a triple point, because it is located where the two borderlines meet [21]. Of course it is an experimental challenge to relate nuclei to this new phase diagram. The IBM dynamical symmetries together with the new critical-point symmetries $E(5)$, $X(5)$ and also $\overline{X(5)}$ are considered to be benchmarks, which are of crucial importance for defining definite observables to classify the different nuclear phases.

In this paper we concentrate on the $X(5)$ symmetry and the region close to it. In the case of the $X(5)$ symmetry the nuclear potential is approximated by a square-well and a harmonic-oscillator potential with respect to the β and γ degrees of freedom, respectively. In addition, the β and γ degrees of freedom are considered to be decoupled. The corresponding Hamiltonian can be solved analytically then, and specific predictions can be made for both the energy spectrum and the transition probabilities [4]. The $X(5)$ energies of the lowest band ($S1$) are located between the vibrator and symmetric-rotor values. As is shown in [22], the gsb energies normalized to the 2^+ band member of the $N = 90$ isotones ^{150}Nd, ^{152}Sm, ^{154}Gd and ^{156}Dy follow the $X(5)$ predictions very well. Crucial observables are also the energy ratios $E(0_2^+)/E(2_1^+)$, $E(4_1^+)/E(2_1^+)$ and $R(4/2)_{S2} = (E(4_2^+) - E(0_2^+))/(E(2_2^+) - E(0_2^+))$. As shown in table 1, for the considered $N = 90$ isotones these quantities also agree very well with the $X(5)$ values. Therefore it is of special interest to check for ^{154}Gd and ^{156}Dy, to which extent the electromagnetic-transition probabilities determined in this work can be reproduced by the $X(5)$ predictions.

Figure 4 shows the Q_t values of the gsb of ^{154}Gd together with the theoretical values of the $X(5)$ symmetry, the symmetric rotor and the IBA $U(5)$ limit [23] normalized to the experimental $Q_t(2^+ \to 0^+)$ value. The $Q_t(4^+ \to 2^+)$ value agrees with the $X(5)$ one. For the states of higher spins the experimental values are just between the $X(5)$ and the rotor values.

Of special importance are also the transition probabilities of the first-excited band ($S2$) and those of the interband transitions between $S1$ and $S2$.

In fig. 5 these quantities as well as the energy spectra of the $X(5)$ $S1$ and $S2$ bands are compared with the corresponding experimental values of ^{154}Gd. The overall agreement is found to be very good for both the energies and the transition probabilities. Note that no fit parameter is used. Only two normalization factors were used, one for the energies and one for the transition probabilities, in order to normalize the energy spectrum to the 2_1^+ energy and the transition probabilities to the $B(E2; 2^+ \to 0^+)$ value. The overall agreement of the experimental values of ^{154}Gd with the $X(5)$ predictions is as good as for ^{150}Nd which was found to be the best example of a $X(5)$ nucleus so far.

Regarding ^{156}Dy the situation looks a bit different. As can be seen in fig. 3, the transition probabilities in the gsb follow those of a symmetric rotor with high precision except the $Q_t(4^+ \to 2^+)$ value which, as in the case of ^{154}Gd, agrees well with the theoretical $X(5)$ value. The experimental values of the β-band or using the $X(5)$ labeling, the $S2$-band, also agree very well with the $X(5)$ predictions up to the first band crossing at spin 12 $\hbar$.

In fig. 6 the experimental energies and transition probabilities of ^{156}Dy are compared with the $X(5)$ predictions and with the results of an IBA [23] fit ($\chi = -0.8\sqrt{7/4}$

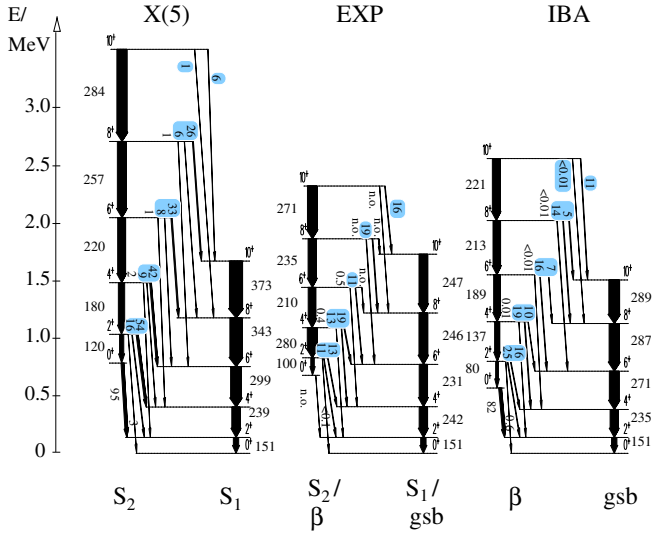

Fig. 6. Comparison of the experimental data of ^{156}Dy with the $X(5)$ predictions and the results of an IBA fit described in the text. The calculated values were normalized as described in the caption of fig. 5.

and $\eta = 0.8$) using the Hamiltonian

$$H = C[\eta n_d - (1-\eta)/N \cdot Q(\chi)Q(\chi)]\,,$$

where

$$n_d = d^\dagger \cdot \tilde{d}$$

and

$$Q(\chi) = (s^\dagger \tilde{d} + d^\dagger s)^{(2)} + \chi \cdot (d^\dagger \tilde{d})^{(2)}.$$

For the determination of the transition probabilities, intensities from [22] were used. It is obvious that the energy spectrum of the $S2$-band of $X(5)$ is more expanded compared to the one of ^{156}Dy, whereas the intra-band transition probabilities agree quite nicely with the $X(5)$ values. The order of magnitude of the inter-band transition probabilities is also in agreement but one specific difference can be observed. In the $X(5)$ symmetry the inter-band transition strengths for the $I_{S2} \rightarrow (I+2)_{S1}$ transitions are larger than for the $I_{S2} \rightarrow I_{S1}$ ones and the $I_{S2} \rightarrow (I-2)_{S1}$ transition strengths are one order of magnitude less than the latter ones. This specific behavior of the inter-band transitions cannot be observed in ^{156}Dy. Here the transition probabilities of the $I_{S2} \rightarrow I_{S1}$ transitions are strongest, whereas the $I_{S2} \rightarrow (I+2)_{S1}$ ones are a bit weaker or have not been observed. In summary, many features of the $X(5)$ symmetry were observed in ^{156}Dy but some deviations, too.

The comparison with the IBA fit gave an overall good description for the energies and the transition strengths. Also the relative strengths of the $I_{S2} \rightarrow (I+2)_{S1}$ to $I_{S2} \rightarrow I_{S1}$ transitions are reproduced.

It is interesting to compare the IBA parameters used in the fit for ^{156}Dy with those reproducing best the $X(5)$ symmetry ($\chi = -1.0\sqrt{7/4}$ and $\eta = 0.75$). This allows to locate ^{156}Dy in the phase diagram of the extended Casten triangle close to the critical point of the $X(5)$ symmetry.

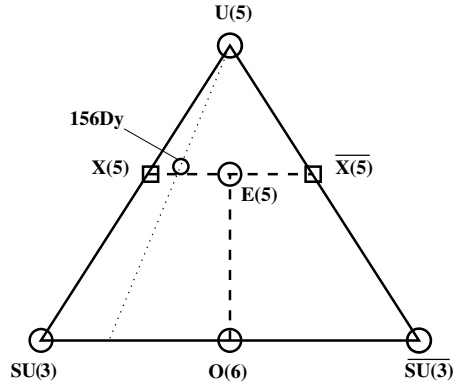

Fig. 7. Extended Casten triangle [20]. The dashed lines represent the lines of first-order phase transitions. The dotted line depicts the $\chi = -0.8\sqrt{7/4}$ line of the IBA parameter space.

Its location is a bit shifted from $X(5)$ towards $O(6)$ (see fig. 7) indicating the onset of γ-softness. This is consistent with the fact that the γ-band of ^{156}Dy is found to be lower in energy as compared to the $N = 90$ isotones ^{150}Nd, ^{152}Sm and ^{154}Gd, all of which are closer to the critical point of the $X(5)$ symmetry.

4 Summary

Precise and reliable lifetimes of excited states in ^{154}Gd were measured using the RDDS technique after Coulomb excitation. Lifetimes in gsb and β-band ($S2$-band) of ^{156}Dy were determined from a coincidence RDDS and a DSAM experiment. Shape changes previously suggested to appear in the gsb of ^{156}Dy and in the s-band above the first band crossing were not supported by the transition probabilities determined in this work. Constant transition quadrupole moments were found in the gsb ($Q_t = 6.1$ eb) as well as in the s-band ($Q_t = 6.5$ eb). A very good agreement is found between experiment and the $X(5)$ predictions in the case of ^{154}Gd. The new experimental data indicate ^{156}Dy to be more γ-soft than the other recently established $X(5)$ nuclei ^{152}Sm and ^{150}Nd. Nevertheless, still many features of a typical $X(5)$ nucleus are observed in ^{156}Dy.

This work was supported by BMBF (Germany) under the contract No. 06OK958 and under the European Union TMR Programme, contract HPRI-CT-1999-00083.

References

1. H. Emling *et al.*, Nucl. Phys. A **419**, 187 (1984).
2. H. Emling *et al.*, Phys. Lett. B **217**, 33 (1989).
3. J.D. Morrison *et al.*, J. Phys. G **15**, 1871 (1989).
4. F. Iachello, Phys. Rev. Lett. **87**, 052502 (2001).
5. R.F. Casten, N.V. Zamfir, Phys. Rev. Lett. **87**, 052503 (2001).
6. R. Krücken *et al.*, Phys. Rev. Lett. **88**, 232501 (2002).

7. T. Klug, A. Dewald, V. Werner, P. von Brentano, R.F. Casten, Phys. Lett. B **495**, 55 (2000).
8. T. Klug, A. Dewald, R.V. Jolos, B. Saha, P. von Brentano, J. Jolie, Phys. Lett. B **524**, 252 (2001).
9. A. Dewald, S. Harissopoulos, P. von Brentano, Z. Phys. A **334**, 163 (1989).
10. NNDC data base, `http//www.nndc.bnl.gov`.
11. G. Böhm *et al.*, Nucl. Instrum. Methods A **329**, 248 (1993).
12. P. Petkov, Nucl. Instrum. Methods A **349**, 289 (1994).
13. P. Petkov *et al.*, Nucl. Phys. A **674**, 357 (2000).
14. H.R. Andrews, D. Ward, R.L. Graham, J.S. Geiger, Nucl. Phys. A **219**, 141 (1973).
15. F. Iachello, Phys. Rev. Lett. **85**, 3580 (2000).
16. R.F. Casten, N.V. Zamfir, Phys. Rev. Lett. **85**, 3584 (2000).
17. J. Jolie, P. Cejnar, J. Dobes, Phys. Rev. C **60**, 0613003 (1999).
18. R.F. Casten, D. Kusnezov, N.V. Zamfir, Phys. Rev. Lett. **82**, 5000 (1999).
19. V. Werner, P. von Brentano, R.F. Casten, J. Jolie, Phys. Lett. B **527**, 55 (2002).
20. J. Jolie, R.F. Casten, P. von Brentano, V. Werner, Phys. Rev. Lett. **87**, 162501 (2001).
21. J. Jolie, P. Cejnar, R.F. Casten, S. Heinze, A. Linnemann, V. Werner, Phys. Rev. Lett. **89**, 182502 (2002).
22. M.A. Caprio *et al.*, Phys. Rev. C **66**, 054310 (2002).
23. F. Iachello, A. Arima, *The Interacting Boson Model* (Cambridge University Press, Cambridge, 1987).